Chapter 19

GMRT Antennas and Feeds

G. Sankar

19.1 Introduction

A radio telescope in its simplest form consists of three components (see also Chapter 3), (i) an antenna that selectively receives radiation from a small region of the sky, (ii) a receiver that amplifies a restricted frequency band from the output of the antenna and (iii) a recorder for registering the receiver output. In this chapter we focus on the antenna, and in particular the antennas used for the GMRT.

The GMRT antennas are parabolic reflector antennas. The first reflector antenna was invented by Heinrich Hertz in 1888 to demonstrate the existence of electromagnetic waves which had been theoretically predicted by J.C.Maxwell. Hertz's antenna was a cylindrical parabola of $f/D = 0.1$ and operated at a wavelength of 66 cm.(450 MHz). The next known reflector antenna was that constructed in 1930 by Marconi for investigating microwave propagation. After that, in 1937, Grote Reber constructed the prototype of the modern dish antenna - a prime-focus parabolic reflector antenna of 9.1 m. diameter, which he used to make the first radio maps of the sky. During and after World War II, radar and satellite communication requirements caused great advances in antenna technology.

19.2 Types of Antennas

A diverse variety of antennas have been used for radio astronomy (see eg. Chapter 3) the principal reason for this diversity being the wide range of observing wavelengths: from ~ 100 m to ~ 1 mm, a range of 10^5. However the most common antenna used for radio astronomy is the paraboloid reflector with either prime-focus feeds or cassegrain type feed arrangement.

Prime-focus parabolic antennas although mechanically simple have certain disadvantages, viz. (i) the image-forming quality is poor due to lower f/D ratios in prime-focus antennas, and (ii) the feed antenna pattern extends beyond the edge of the parabolic reflector and the feed hence picks up some thermal radiation from ground. The cassegrain system which uses a secondary hyperboloid reflector and has the feed located at the second focus of the secondary solves these problems. For cassegrain systems the f/D ratio is higher and further the feed "looks" upwards and hence pick up from the ground is minimized. This is a great advantage at higher frequencies, where the ground brightness temperature (~ 300 K) is much higher than the brightness temperature of the sky. However this is achieved at the price of increased aperture blockage caused by the secondary reflector.

A primary advantage of paraboloid antennas (prime focus or cassegrain) is the ease with which receivers can be coupled to it. The input terminals are at the feed horn or dipole. A few other advantages are: (i) high gain, a gain of $\simeq 25$ dB for aperture diameters as small as 10λ is easily achievable, (ii) full steerability, generally either by polar or azimuth-elevation mounting. Further the antenna characteristics are to first order independent of pointing, (iii) operation over a wide range of wavelengths simply by changing the feed at the focus.

Compared to optical reflectors paraboloid reflectors used for radio astronomy generally have a short f/D ratio. Highly curved reflectors required for higher f/D ratios result in increased costs and reduced collecting areas. Although the reflecting antennas are to first order frequency independent, there is nonetheless a finite range of frequencies over which a given reflector can operate. The shortest operating wavelength is determined by the surface smoothness of the parabolic reflector. If λ_{mn} is the shortest wavelength,

$$\lambda_{mn} \approx \sigma/20 \tag{19.2.1}$$

where, σ is the rms deviation of the reflector surface from a perfect paraboloid. Below λ_{mn} the antenna performance degrades rapidly with decreasing wavelength. The longest operating wavelength λ_{mx}, is governed by diffraction effects. As a rule of thumb the largest operating wavelength λ_{mx} is given by

$$\lambda_{mx} \ < \ 2\bar{L} \tag{19.2.2}$$

where, $\bar{L}$ is the mean spacing between feed–support legs. At $\lambda = \bar{L}$ the feed support structure would completely shadow the reflector.

19.3 Characterizing Reflector Antennas

One important property of any antenna is that its radiation characteristics when it is used as a transmitter are the same as when it is in the receiving-mode. This is a consequence of the well-known electromagnetic fields *principle of reciprocity*. Even though radio telescope antennas are generally used only for receiving signals, it is often simpler to characterize it by considering the antenna to be in the transmitting mode. Antenna terminology is also influenced by the reciprocity principle, for example we have been calling the dipole or horn placed at the focus of the reflector to receive the signal from distant sources as the "**feed**", i.e. as though it were coupled to a transmitter rather than a receiver.

All antennas can be described by the following characteristics (see also Chapter 3)

1. Radiation pattern The field strength that the antenna radiates as a function of direction. The simplest type of antenna normally radiates most of its energy in one direction called the 'primary beam' or 'main lobe'. The angular width of the main lobe is determined by the size and design of the antenna. It is usually parametrized by its full width at half maximum, also called its 3dB beamwidth. Weaker secondary maxima in other directions are called *side lobes*. Although the pattern is a function of both elevation and azimuth angle, it is often only specified as a function of elevation angle in two special orthogonal planes, called the E-plane and the H-plane.

2. Directivity The radiated power in the direction of the main lobe relative to what would be radiated by an isotropic antenna with the same input power. A related quantity

called the Gain also takes into account any electrical losses of the antenna. For reflector antennas, one can also define an aperture efficiency which is the ratio of the effecting collecting area of the telescope to its geometric area. For the relation between the gain and the effective collecting area see Chapter 3.

3. Polarization The sense of polarization that the antenna radiates or receives as a function of direction. This may be linear, circular, or elliptical. Note that when describing the polarization of a wave, it is sufficient to specify the polarization of the electric-field vector.

4. Impedance From the point of view of the microwave circuit behind the antenna, the antenna can be represented as a complex load impedance. The characteristics of this load depend on the radiation patterns of the antenna and hence the design of the antenna. The goal of a good design is to match the impedance of the antenna to the impedance of the transmission line connecting the antenna to the receiver. The impedance match can be characterized by any one of the following parameters:

   - the voltage reflection coefficient, ρ_v.
   - the return loss (in dB), $R_L = -20\log|\rho_v|$.
   - the voltage standing-wave ratio, $VSWR = \frac{1+|\rho_v|}{1-|\rho_v|}$.

5. Phase Center All horns and feeds have a *phase center*. This is the theoretical point along the axis of the feed which is the center of curvature of the phase fronts of the emerging spherical waves.

19.4 Computing Reflector Antenna Radiation Patterns

Reflector antenna radiation patterns are determined by a number of factors, but the most important ones are the radiation pattern of the feed antenna and the shape of the reflector. Parabolic reflectors have the unique feature that all path lengths from the focal point to the reflector and on to the aperture plane are the same. As shown in Figure 19.1,

$$\begin{aligned} FP + PA &= \rho + \rho\cos\theta' \\ &= \rho(1+\cos\theta') \\ &= 2f, \end{aligned} \tag{19.4.3}$$

since the parabola is described in polar form by, $\rho(1+\cos\theta') = 2f$

When the reflector dimensions are large compared to the wavelength, geometrical optics principles can be used to determine the power distribution in the aperture plane. If the feed pattern is azimuthally symmetric, then the normalized far-field radiation pattern of reflector depends on

1. $\pi u = k\ a\ \sin\theta$, where a is the radius of the aperture, $k = 2\pi/\lambda$, and θ is the angle subtended by the far-field point with respect to the parabola's focal axis

2. The feed taper,C [4],[5], which is defined as the amplitude of the feed radiation pattern at the rim of the parabolic reflector relative to the maximum value (assumed to be along the parabola axis). (Note that in standard power plots of radiation patterns (in dB), the edge taper T_E is related to C by $T_E = 20\log C$).

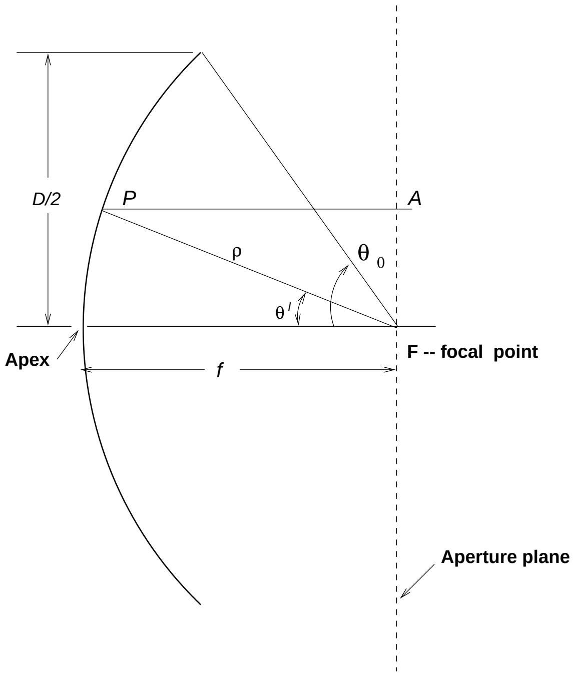

Figure 19.1: Geometry for determining the aperture field distribution for a prime focus parabolic antenna.

3. The focal length f which determines how the power from the feed is spread over the aperture plane. If $\tilde{g}(\theta')$ is the radiation pattern of the feed, r is distance in the aperture plane, and $g(r)$ is the power density in the aperture plane, then we have

$$g(r)\ dr = \tilde{g}(\theta')\ d\theta',\ \text{i.e. } g(r) = \tilde{g}(\theta')\ \frac{d\theta'}{dr} \tag{19.4.4}$$

and from Figure 19.1 we have

$$\frac{d\theta'}{dr} = \frac{2f}{1 + cos(\theta')} \tag{19.4.5}$$

In Chapter 3 we saw that the far field is in general the Fourier transform of the aperture plane distribution. In the case of azimuthally symmetric distributions, this can be written as

$$F(u) \quad = \quad \int_0^{\pi} g(q) J_0(qu) q\, dq$$

where $F(u)$ is the far field pattern, q is a normalized distance in the aperture plane, $q = \pi(r/a)$, $g(q)$ is the feed's pattern projected onto the aperture plane as discussed above. A convenient parameterization of the feed pattern in terms of the taper, C is

$$g\left(\frac{r}{a}\right) \quad = \quad C + (1 - C)\left[1 - \left(\frac{r}{a}\right)^2\right]^n \tag{19.4.6}$$

$$\tag{19.4.7}$$

The aperture illuminations corresponding to different values of the parameter n are shown in Figure 19.2. The case $n = 0$ corresponds to a uniform aperture distribution.

For uniform illumination the far field pattern is given by

$$F(u) = 2 \cdot \frac{J_1(\pi u)}{(\pi u)} \tag{19.4.8}$$

Simple closed-form expressions are available for integer values of n. If the above expression $F(u)$ is denoted as $F_0(u)$, (since $n = 0$) the general form for any integer n is given by

$$F_n(u) \quad = \quad \frac{n+1}{Cn+1} \cdot \left[C F_0(u) + \frac{1-C}{n+1} f_n(u)\right] \tag{19.4.9}$$

where,

$$f_n(u) \quad = \quad 2^{n+1}(n+1)! \frac{J_{n+1}(\pi u)}{(\pi u)^{n+1}} \tag{19.4.10}$$

Table 19.1 gives the halfpower beamwidth (HPBW), the first sidelobe level and the taper efficiency (see Section 19.4.1) for various edge tapers C and shape parameter n.

From Table 19.1 (see also the discussion in Chapter 3) we find that as the edge-taper parameter C decreases, the HPBW increases, the first sidelobe level falls and the taper-efficiency also decreases. Note that C has to be less than unity since we have assumed a radiation pattern which decreases monotonically with increasing angle from the symmetry-axis (Eqn 19.4.6, Fig 19.2).

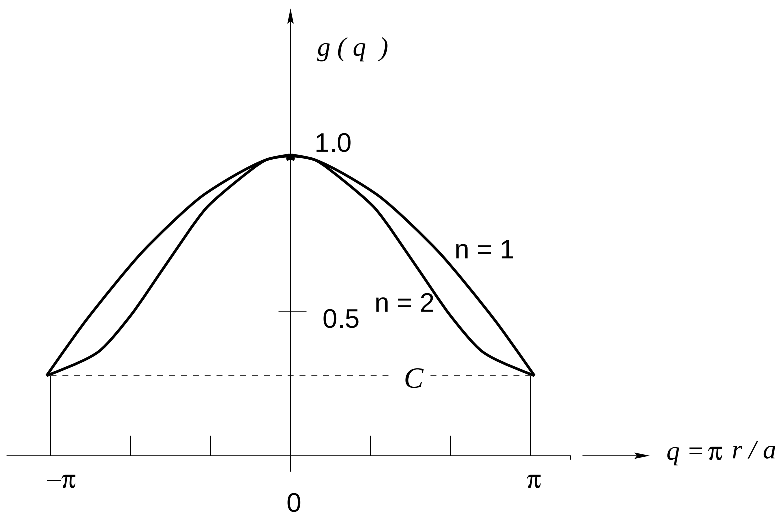

Figure 19.2: The shape of the aperture illumination as given by eqn 19.4.6 for different values of the parameter n.

Table 19.1: Radiation characteristics of circular aperture

Edge Taper		$n = 1$			$n = 2$		
T_E (dB)	C	HPBW (rad.)	Sidelobe level (dB)	η_t	HPBW (rad.)	Sidelobe level (dB)	η_t
-8	0.398	$1.12\lambda/2a$	-21.5	0.942	$1.14\lambda/2a$	-24.7	0.918
-10	0.316	$1.14\lambda/2a$	-22.3	0.917	$1.17\lambda/2a$	-27.0	0.877
-12	0.251	$1.16\lambda/2a$	-22.9	0.893	$1.20\lambda/2a$	-29.5	0.834
-14	0.200	$1.17\lambda/2a$	-23.4	0.871	$1.23\lambda/2a$	-31.7	0.792
-16	0.158	$1.19\lambda/2a$	-23.8	0.850	$1.26\lambda/2a$	-33.5	0.754
-18	0.126	$1.20\lambda/2a$	-24.1	0.833	$1.29\lambda/2a$	-34.5	0.719

19.4.1 Aperture Efficiency

The "aperture efficiency" of an antenna was earlier defined (Sec 19.3) to be the ratio of the effective radiating (or collecting) area of an antenna to the physical area of the antenna. The aperture efficiency of a feed-and-reflector combination can be decomposed into five separate components: (i) the illumination efficiency or "taper efficiency", η_t, (ii) the spillover efficiency, η_S, (iii) the phase efficiency, η_p, (iv) the crosspolar efficiency, η_x and (v) the surface error efficiency η_r.

$$\eta_a = \eta_t \, \eta_S \, \eta_p \, \eta_x \, \eta_r. \tag{19.4.11}$$

The illumination efficiency (see also Chapter 3, where it was called simply "aperture efficiency") is a measure of the nonuniformity of the field across the aperture caused by the tapered radiation pattern (refer Figure 19.2). Essentially because the illumination is less towards the edges, the effective area being used is less than the geometric area of the reflector. It is given by

$$\eta_t = \frac{|\int_0^R g(r)dr|^2}{\int_0^R |g(r)|^2 dr}, \tag{19.4.12}$$

where $g(r)$ is the aperture field. Note that this has a maximum value of 1 when the aperture illumination is uniform, i.e. $g(r) = 1$. The illumination efficiency can also be written in terms of the electric field pattern of the feed $E(\theta)$, viz.

$$\eta_t = 2\mathrm{cot}^2 \frac{\theta_0}{2} \cdot \frac{|\int_0^{\theta_0} E(\theta)\tan(\theta/2)d\theta|^2}{\int_0^{\theta_0} |E(\theta)|^2 \sin(\theta)d\theta}, \tag{19.4.13}$$

where θ_0 is angle subtended by the edge of the reflector at the focus (Figure 19.1).

When a feed illuminates the reflector, only a proportion of the power from the feed will intercept the reflector, the remainder being the spillover power. This loss of power is quantified by the spillover efficiency, i.e.

$$\eta_S = \frac{\int_0^{\theta_0} |E(\theta)|^2 \sin(\theta)d\theta}{\int_0^{\pi} |E(\theta)|^2 \sin(\theta)d\theta}. \tag{19.4.14}$$

Note that the illumination efficiency and the spillover efficiency are complementary; as the edge taper increases, the spillover will decrease (and thus η_S increases), while the illumination or taper efficiency η_t decreases[1] The tradeoff between η_S and η_t has an optimum solution, as indicated by the product η_S * η_t in Figure 19.3. The maximum of $\eta_S\eta_t$ occurs for an edge taper of about -11 dB and has a value of about 80 %. In practice, a value of -10 dB edge taper is frequently quoted as being optimum.

The surface-error efficiency is independent of the feed's illumination. It is associated with far-field cancellations arising from phase errors in the aperture field caused by errors in the reflector's surface. If δ is the rms error in the surface of the reflector, the surface-error efficiency is given by

$$\eta_r = \exp -(4\pi\delta_p/\lambda)^2 \tag{19.4.15}$$

The remaining two efficiencies, the phase efficiency and the cross polarization efficiency, are very close to unity; the former measures the uniformity of the phase across

[1] Recall also from Chapter 3 that as the illumination is made more and more uniform the sidelobe level increases.

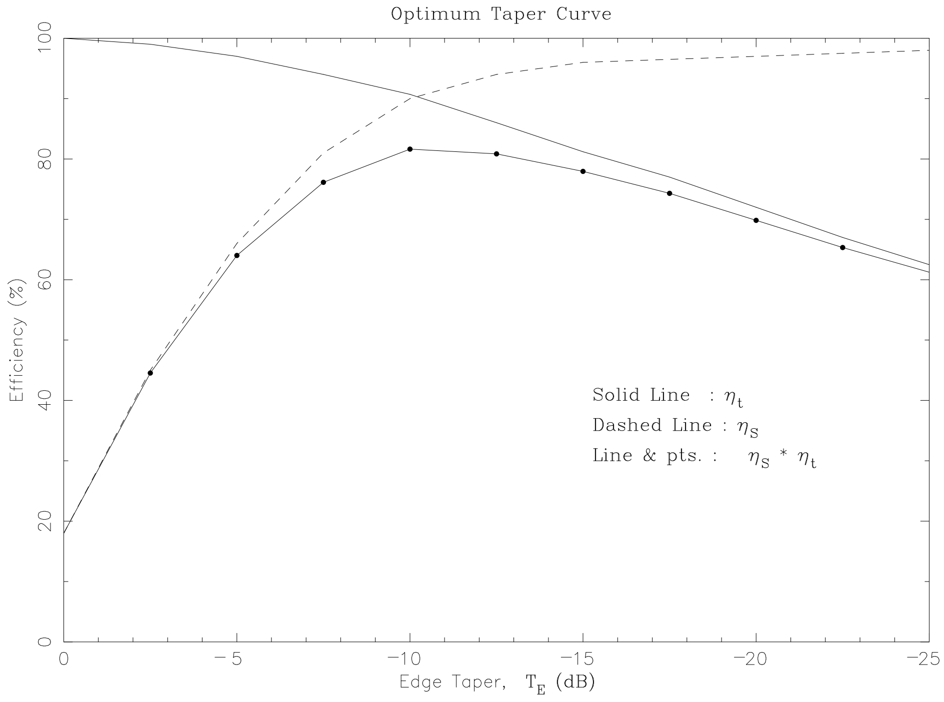

Figure 19.3: Illumination efficiency and spillover efficiency as a function of edge taper. The optimum taper is at ~ -11 dB.

the aperture and the latter measures the amount of power lost in the cross-polar radiation pattern. For symmetric feed patterns[6], η_x is defined thorough the copolar,$C_p(\theta)$ and cross-polar patterns,$X_p(\theta)$:

$$\eta_x = \frac{\int_0^{\theta_0} |X_p(\theta)|^2 \sin(\theta) d\theta}{\int_0^{\theta_0} (|C_p(\theta)|^2 + |X_p(\theta)|^2) \sin(\theta) d\theta} \tag{19.4.16}$$

where,

$$\begin{aligned} C_p(\theta) &= 1/2[E(\theta) + H(\theta)] \\ X_p(\theta) &= 1/2[E(\theta) - H(\theta)] \end{aligned} \tag{19.4.17}$$

It can be seen that if one can design an antenna,having identical $E(\theta), H(\theta)$ patterns the cross-polar pattern will vanish. Taking the cue from this, *the feed for antenna could also designed with a goal to match E and H patterns at least up to the subtended angle of the dish edge*, θ_0.

With this background we now proceed to take a detailed look at the GMRT antennas.

19.5 Design Specifications for the GMRT Antennas

The f/D ratio for the GMRT antennas was fixed at the value 0.412 based both on structural design issues as well as preliminary studies of various feeds radiation patterns. Since the antennas are to work at meter wavelengths prime focus feeds were preferred. Cassegrain feeds at meter wavelengths would result in impractically large secondary mirrors (the mirror has to be several λ across) and concomitant large aperture blockage.

Six bands of frequencies had been identified [1] for the GMRT observations. It was deemed essential to be able to change the observing frequency rapidly, and consequently the feeds had to mounted on a rotating turret placed at the prime focus. If one were to mount all the six feeds on a rotating hexagon at the focus, the adjacent feeds will be separated by $60°$. If one wants to illuminate the entire aperture, then one has to have a feed pattern that extends at least up to the subtended angle of the parabola edge, which is $\theta_0 = 62.5°$ (Note that $\cot(\theta_0/2) = 4f/D$, Figure 19.1). Hence this arrangement of feeds would cause the one feed to "see" the feeds on the adjacent faces. It was decided therefore to mount the feeds in orthogonal faces of a rotating cube. Since one needs six frequency bands, this leads to the constraint that at least two faces of the turret should support dual frequency capability. For astronomical reasons also dual frequency capability was highly desirable.

One specific aspect of GMRT design is the use of mesh panels to make the reflector surface[1]. Since the mesh is not perfectly reflective, transmission losses thorough the mesh have to be taken into account. Further, the expected surface errors of the mesh panels was ~ 5 mm. This implies that the maximum usable frequency is (see Section 19.2) ~ 3000 MHz, independent of the transmission losses of the mesh. (Incidentally, since the mean-spacing of feed-support legs, $\bar{L} = 23.6$ m, the lowest usable frequency is around 6 MHz).

Several analytical methods exist in literature to compute the transmission loss through a mesh as a function of the cell size, the wire diameter and the wavelength of the incident radiation. The one chosen for our application is has good experimental support [2,3]. At the GMRT, the mesh size is 10×10 mm for the central 1/3 of the dish, 15×15 mm of the

Mesh size	$\lambda = 21$ cm.	$\lambda = 50$ cm.
10 mm.	-15.8 dB	-23.3 dB
15 mm.	-11.4 dB	-18.4 dB
20 mm.	-8.1 dB	-14.6 dB

Table 19.2: Transmission losses through the GMRT wire mesh

middle 1/3 of the dish and 20×20 mm for the outer 1/3 of the dish. The wire diameter is 0.55 mm. The transmission loss for at two fiducial wavelengths for these various mesh sizes is given in Table 19.2.

Each section of the dish not only has a separate mesh size but also a separate surface rms error. If we call these rms surface errors $\sigma_1, \sigma_2, \sigma_3$ and the respective transmission losses (at some given wavelength) τ_1, τ_2, τ_3, then the surface rms efficiency given by Eqn 19.4.15 has to be altered to a weighted rms efficiency:

$$\eta_r = \frac{A_1 + A_2 + A_3}{\int_0^{\theta_0} |E(\theta)|^2 \sin(\theta) d\theta}$$

where,

$$A_1 = \exp\left[-\left(\frac{4\pi\sigma_1}{\lambda}\right)^2\right] \int_0^{\theta_2} |E(\theta)|^2 \sin(\theta) d\theta \quad (19.5.18)$$

$$A_2 = \exp\left[-\left(\frac{4\pi\sigma_2}{\lambda}\right)^2\right] \int_{\theta_2}^{\theta_1} |E(\theta)|^2 \sin(\theta) d\theta \quad (19.5.19)$$

$$A_3 = \exp\left[-\left(\frac{4\pi\sigma_3}{\lambda}\right)^2\right] \int_{\theta_1}^{\theta_0} |E(\theta)|^2 \sin(\theta) d\theta \quad (19.5.20)$$

and θ_2, θ_1 are the subtended angles of the first and second points of mesh–transition–zones, as illustrated in Figure 19.4

The transmission loss gives a corresponding mesh–leakage or *mesh–transmission* efficiency,η_{mt}, which is given by

$$\eta_{mt} = \frac{B_1 + B_2 + B_3}{\int_0^{\theta_0} |E(\theta)|^2 \sin(\theta) d\theta} \quad (19.5.21)$$

where,

$$B_1 = (1 - \tau_1) \int_0^{\theta_2} |E(\theta)|^2 \sin(\theta) d\theta \quad (19.5.22)$$

$$B_2 = (1 - \tau_2) \int_{\theta_2}^{\theta_1} |E(\theta)|^2 \sin(\theta) d\theta \quad (19.5.23)$$

$$B_3 = (1 - \tau_3) \int_{\theta_1}^{\theta_0} |E(\theta)|^2 \sin(\theta) d\theta \quad (19.5.24)$$

Efficiencies computed for the different GMRT feeds (using their measured pattern, being the input) are given in Table 19.4.

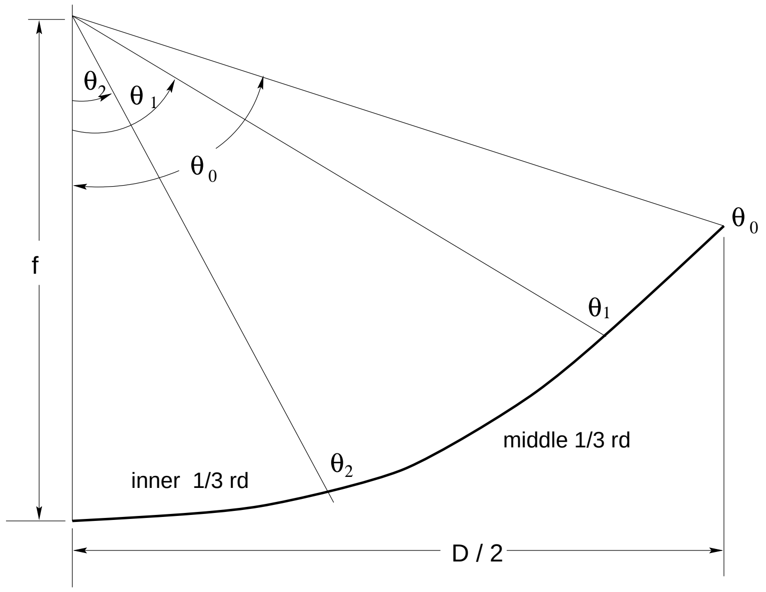

Figure 19.4: Schematic of the sub division of the GMRT antenna surface into 3 zones. The mesh size as well as the rms surface error is different in the different zones.

19.5.1 Secondary Patterns

The antenna pattern at 327 MHz as computed using geometric optics is shown in Figure 19.5. More rigorous analytical models (the *Uniform Theory of Diffraction* [7]) gives the pattern shown in Figure 19.6.

There is a pronounced difference seen at the side–lobe structures between these two models, while the primary beam shows near–identical shapes and the HPBW value matches to a second decimal accuracy. The computed HPBW also agrees to within measurement errors with the observed HPBW of the actual GMRT antennas.

19.6 GMRT Feeds

19.6.1 Feed Placement

Recall that from the constraints outlined in Sec 19.5 it had been decided that the feed turret should be cubical in shape. Fig 19.7 shows the placement of feeds on the turret. The phase–centers of all the feeds are coincident with the paraboloid focus. The space between the turret and the feed is utilized for mounting the front-end electronics. There are six bands altogether, $1000 - 1450$ MHz[2], 610 MHz, 327 MHz, 233 MHz, 150 MHz and 50 MHz. The 50 MHz feed[3] is affixed onto the feed support legs and not onto the turret. As such it is in focus at all times. The 610 MHz and 233 MHz feeds are mounted on the same turret face.

Each type of feed - its design and performance are briefly outlined in the following sections. More information can be found in [8].

[2]Note that some of the antennas have feeds that extend to 1750 MHz.

[3]Which is not yet operational

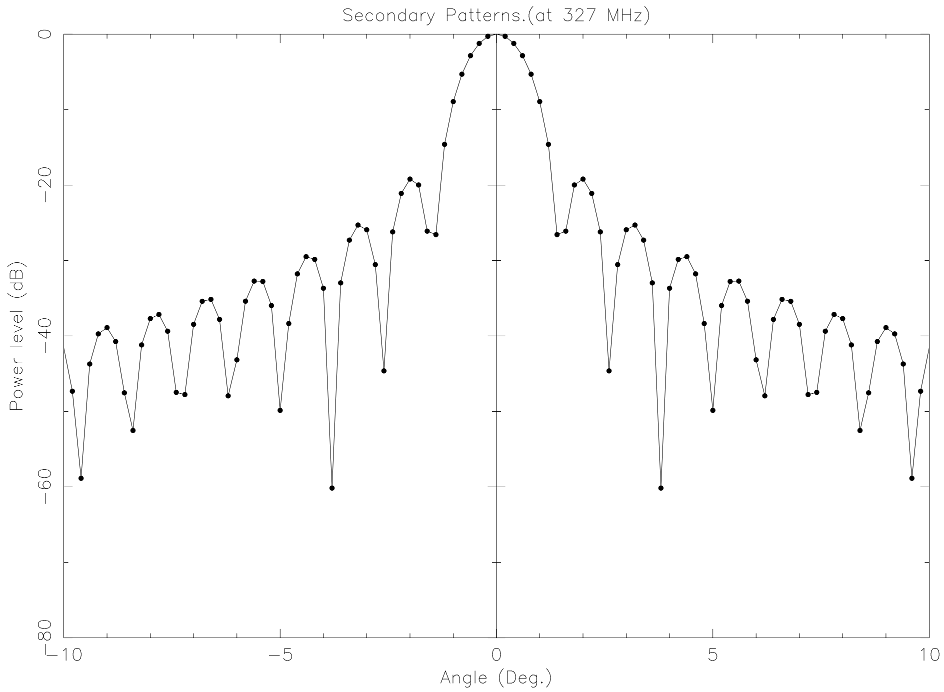

Figure 19.5: Computed pattern (using geometric optics) of a GMRT antenna at 327 MHz.

19.6.2 150 MHz Feed

This feed employs four dipoles in a "boxing ring" configuration, placed above a plane reflector. The unique feature of the dipole is that it is wide-band i.e. has an octave bandwidth. It is a folded dipole with each arm being a "*thick*" dipole. A dipole is called '*thin*' when its diameter, $d > 0.05\lambda$. For such dipoles a sinusoidal current distribution can be assumed for the computation of input impedance and related radiation parameters.

Thin dipoles have narrowband radiation characteristics. One method by which its acceptable operational bandwidth can be increased is to decrease the l/d ratio. For example, an antenna with a $l/d \approx 5000$ has an acceptable bandwidth of about 3%, while an antenna of the same length but with a $l/d \approx 260$ has a bandwidth of about 30%. By folding the dipole, one gets a four–fold increase in input impedance compared to a simple dipole. The 150 MHz feed also has a transmission line impedance transformer coupled to the excitation point [9].

Traditionally crossed–dipoles are used to give sensitivity to both polarizations. However since a crossed–dipole configuration in this design would be extremely cumbersome, a "boxing ring" design was instead chosen. Here one pair of dipoles at $\lambda/2$ spacing provides sensitivity to one linear polarization. Another pair orthogonally oriented with respect to the first pair gives sensitivity to the orthogonal polarization. The overall dimensions of the feed are:

- Folded dipole length : $0.39\,\lambda$

- Dipole height above reflector : $0.29\,\lambda$

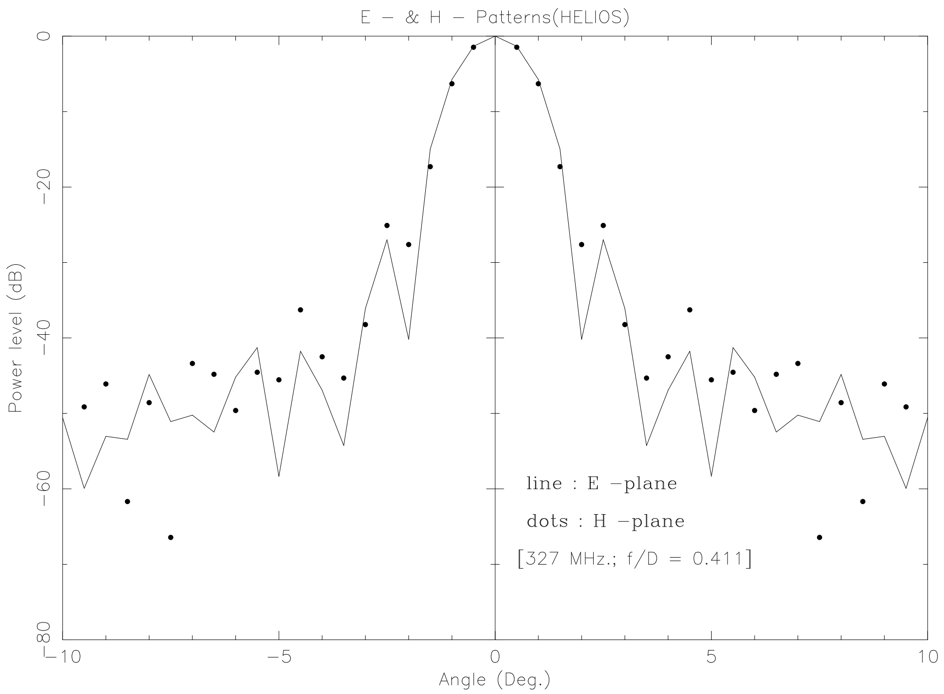

Figure 19.6: Computed pattern (using uniform theory of diffraction) of a GMRT antenna at 327 MHz.

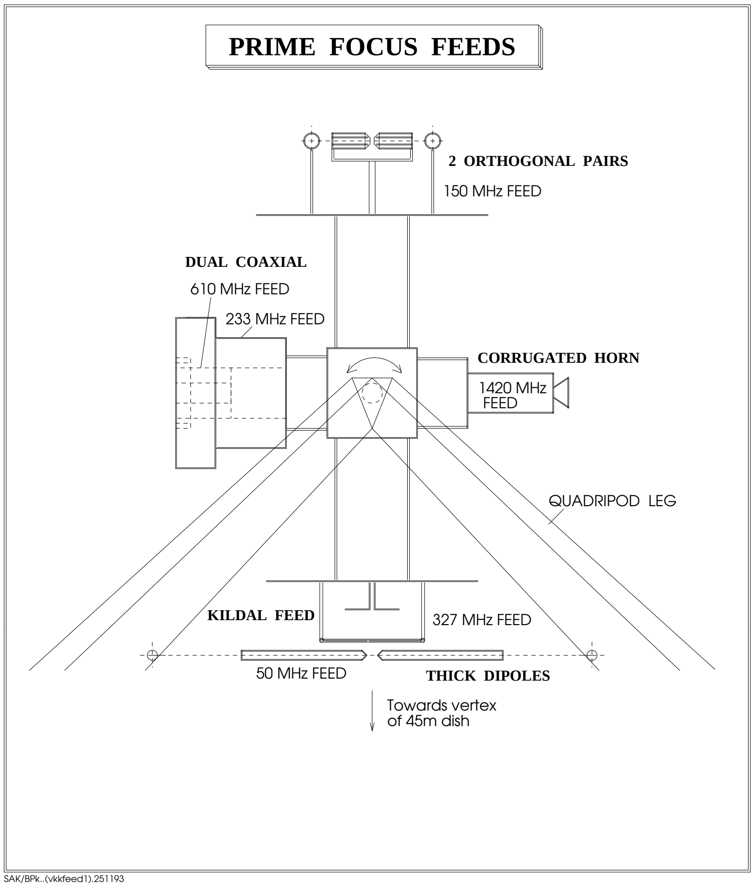

Figure 19.7: Schematic diagram showing the arrangement of the different feeds on the feed turret.

- Reflector (diagonal of octagon) : $1.2\ \lambda$

The dipoles have an l/d ratio of 6.48, and the phase center was determined to be at a height of 100 mm above the reflector. The feed's impedance bandwidth can be seen on the VSWR plot of Figure 19.8

The usable bandwidth for a feed is given approximately by the range for which SWR ≤ 2.0. By this criteria, the frequency coverage of the 150 MHz feed is from 117 MHz to 247 MHz, i.e. a bandwidth of 130 MHz, or 86% bandwidth. The radiation pattern gives an edge taper, $T_E = -9$ dB.

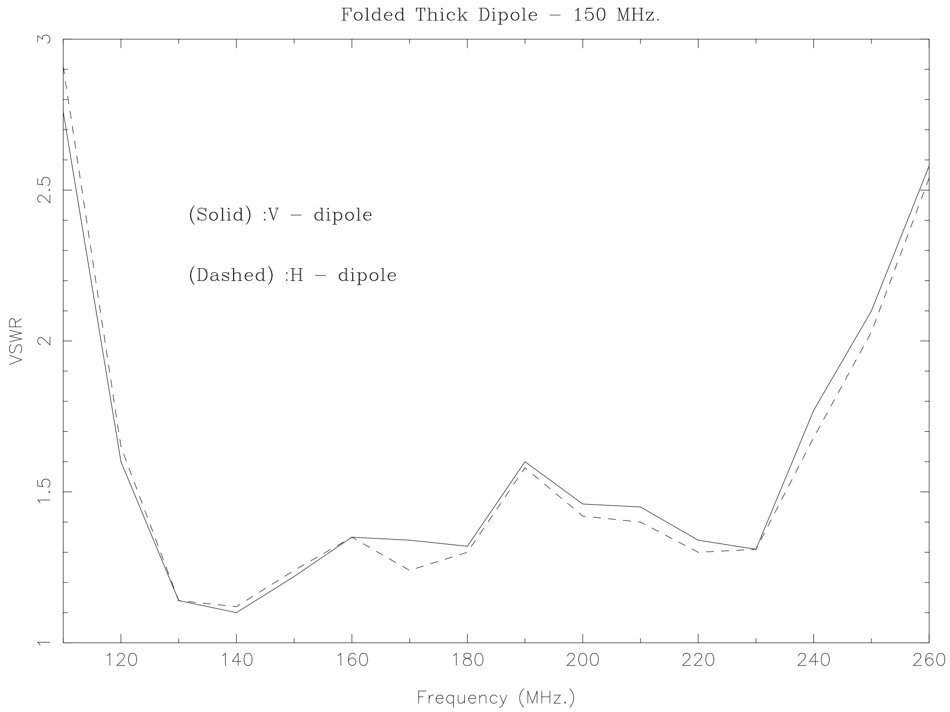

Figure 19.8: VSWR for the 150 MHz feed.

One undesirable feature of this feed is the high value of cross–polarization, as compared to that at other frequencies (see Figure 19.9)[4]. The cross–polar peak for 150 MHz. is -17 dB and the on–axis cross polarization is also at about the same level.

One–pair of outputs from the dipoles which are parallel to each other are connected to a power–combiner, whose output goes to one port of the quadrature hybrid (which adds two linear polarized signals to yield one circular polarized signal). Similarly the orthogonal pair of dipoles are connected to the other port of the hybrid. Both the power combiners and the quadrature hybrid are mounted inside one of the front-end chassis, placed behind the feed.

19.6.3 327 MHz Feed

Generally a dipole has a broader H pattern than its E pattern (the E pattern being in the plane containing the dipole). Recall from the discussion in section 19.4.1 that for good cross–polarization properties it was essential to have matched E and H plane patterns. An elegant method for achieving this pattern matching was given by P.S.Kildal [10], and involves placing a *beam forming ring* (BFR) above the dipole[5]. The conducting ring is placed above the dipole in a plane parallel to the reflector and is supported by dielectric rods. The beam forming ring compresses the H-plane pattern while it has no significant effect on the E-plane.

[4]Note that the cross polar pattern was measured using the standard technique outlined in [4 ; pp.177–79]. The cross–polar levels are measured with respect to a co–polar maximum of 0 dB.

[5]This design has been christened '*Kildal Feed*' in the local jargon.

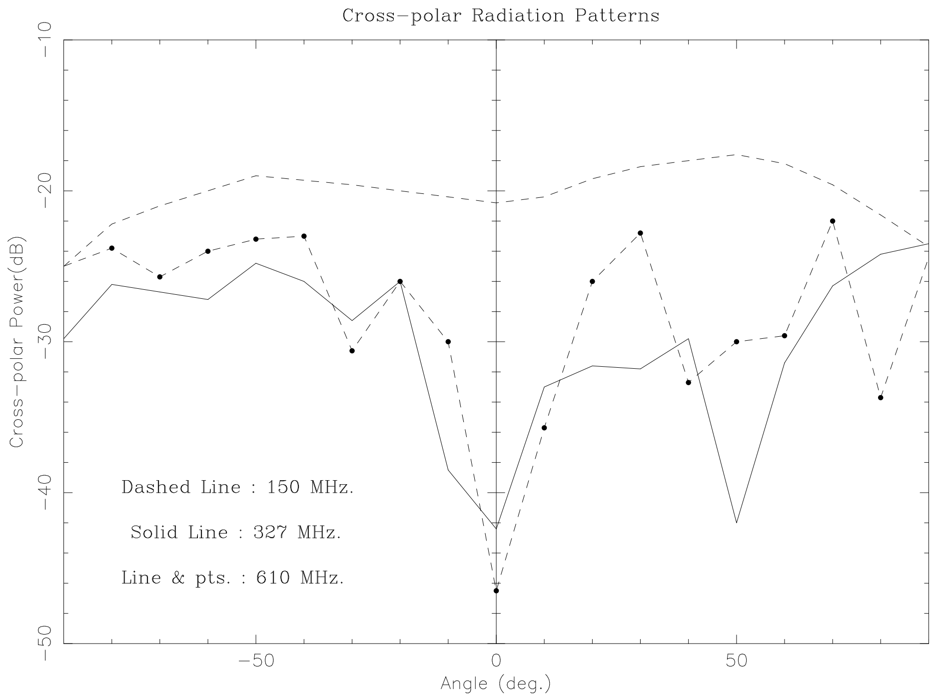

Figure 19.9: The cross polarization of different GMRT feeds. The 150 MHz feed has relatively larger cross-polarization.

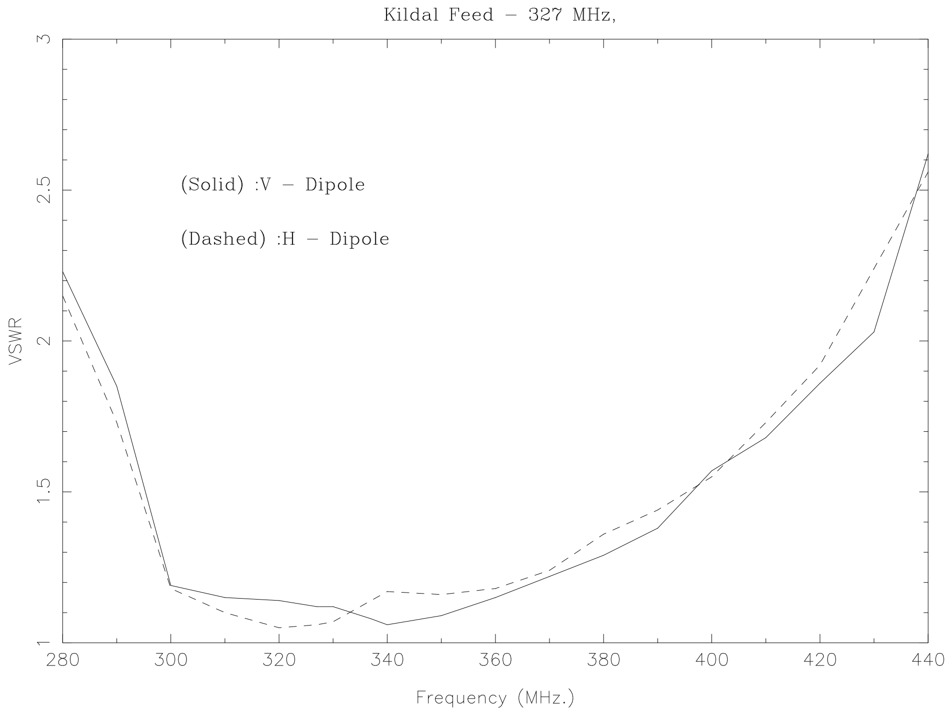

Figure 19.10: The VSWR as a function of frequency for the 327 MHz feed.

The optimum dimensions of the dipole, BFR and reflector were arrived at by careful measurements done on a scaled-up version (i.e. at 610 MHz) and a follow–up measurements on a prototype 327 MHz model. The values arrived at were :

- Reflector diameter : 2.2λ.
- Height of dipole above reflector : 0.26λ.
- BFR diameter : 1.22λ.
- BFR height above reflector : 0.51λ.

The measured phase center is at 26 mm above the reflector for both E and H- planes. Crossed dipoles are employed for dual polarization. The 327 MHz feed actually deviates slightly from the original Kildal's design – there are sleeves over the dipoles. These sleeves increase the bandwidth of the feed [5]. The VSWR plot for the 327 MHz feed is given in Figure 19.10.

For SWR ≤ 2.0, the bandwidth is 138 MHz.(286 to 424 MHz.) The measured antenna pattern is given in Fig 19.11. The edge taper, T_E is -12.2 dB. Fig 19.9 shows the cross-polar pattern. It is seen that a cross-polar maximum of -27.5 dB (mean value) has been achieved.

The linear polarized outputs of the dipoles are mixed in a quadrature hybrid at one of the front-end chassis to produce two circular polarized (both left and right) signals, which go further into the amplifying, signal conditioning circuits of front-end Electronics.

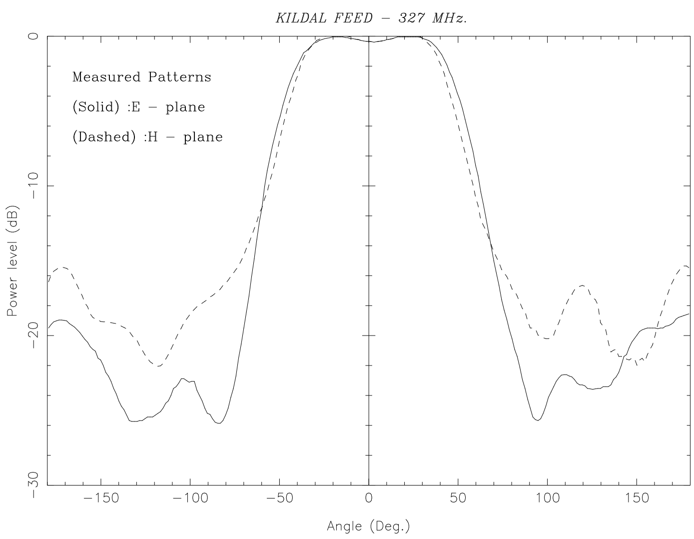

Figure 19.11: The measured antenna pattern at 327 MHz

19.6.4 Dual-Frequency Coaxial Waveguide Feed

The 610 MHz and 233 MHz feeds are dual frequency coaxial feeds. The single most attractive feature of coaxial waveguide feed is its' multi-frequency launching capability. Simultaneous transmission or reception of well separated frequencies is possible. Coaxial feeds have been used as on board satellite antennas to provide coverage at three separate frequency bands [11]. Coaxial feeds have also been used at the WSRT (operated by NFRA, The Netherlands). The prime focus feed system has at WSRT has two separate multi-frequency coaxial waveguides, covering 327 MHz, 2300 MHz in one and 610 MHz, 5000 MHz in another [12],[13].

The design of the GMRT 610 MHz/233 MHz waveguide feeds is based on an exhaustive theoretical analysis of the design of coaxial waveguide feeds [14],[15]. A constraint in such multi-frequency designs is that adjacent frequency bands should not overlap to within an octave. Thus at the GMRT either the 150 MHz or the 233 MHz could have been combined with 610 MHz. However the former choice was rejected since it resulted in unwieldy dimensions of the feed.

The fundamental mode of propagation in coaxial structures is TEM, hence the radiated field component along the axis is zero everywhere. Obviously for a feed this is the most undesirable characteristic. So propagation by an alternate mode (single or multiple) is essential. Coaxial waveguides must then be forced to radiate in TE_{11} mode. This can be achieved simply by exciting the probes in phase opposition[6].

In the dual frequency construction the outer conductor of the 610 MHz serves as the inner one for the 233 MHz. Quarter wavelength chokes are provided in both the frequency

[6]Low loss baluns are essential in such designs.

Dimensions	*610 MHz Coaxial*	*233 MHz Coaxial*
Aperture diameter	$0.9\,\lambda$	$0.85\,\lambda$
Waveguide cavity length	$0.95\,\lambda$	$0.73\,\lambda$

Table 19.3: Dimensions of the 610/233 MHz coaxial feed.

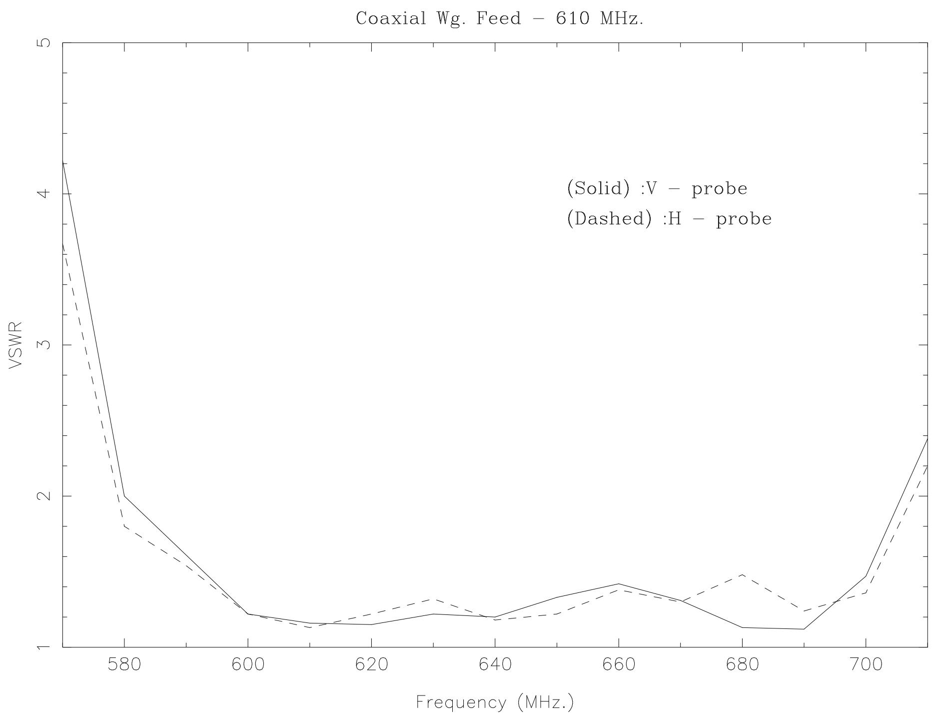

Figure 19.12: The VSWR as a function of frequency for the 610 MHz feed.

parts to cut down the surface currents on the outer conductor and thereby ensure pattern symmetry. The waveguide feeds have two pairs of probes. One pair supports a given plane polarization while the orthogonal pair supports the orthogonal polarization. Similar to the dipole feed discussed in the previous section, a quadrature hybrid at the back-end of the coaxial feed is used to convert the linear polarization to circular polarization. The rear-half of the 610 MHz feed, separated by a partition disc, is utilized to accommodate the baluns, quadrature hybrids and low-noise amplifiers of 610 MHz and the baluns of 233 MHz. The overall dimensions of the feed are given in Table 19.3

The phase center is not at the aperture plane, but at a point 60 mm in front of the aperture. A similar displacement of the phase center is also seen in the WSRT coaxial feeds [13]. Fig 19.12 shows the VSWR plot for an optimized probe geometry at 610 MHz For SWR ≤ 2.0, the band goes from 580 MHz to 707 MHz, i.e. a total bandwidth of 127 MHz. The feed patterns measured at 610 MHz are shown in Fig 19.13; the edge taper is -9.8 dB. The cross-polar maximum is -22.8 dB.

Fig 19.14 shows the VSWR plot of 233 MHz– part of the coaxial feed.

For SWR ≤ 2.0, the bandwidth is 12 MHz, i.e. this feed is rather narrow as compared to all other frequency bands. The effect of the inter-coupling of radiated power between

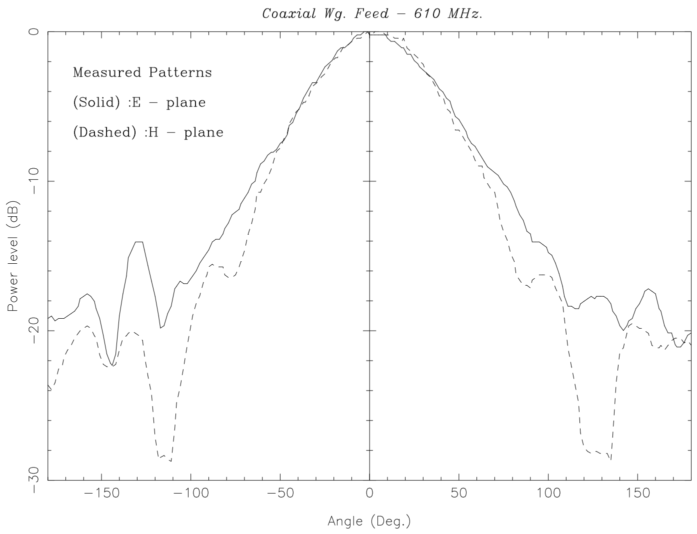

Figure 19.13: The feed pattern of the 610 MHz feed.

the two frequencies of the coaxial feed on the radiation patterns has been studied. The main lobe does not show any significant change due to the presence of the other coaxial waveguide part.

19.7 1000–1450 MHz Feed

This feed was designed and constructed by the Millimeter Wave Laboratory of the Raman Research Institute. It is of the corrugated horn type - known for its high aperture efficiency and very low cross-polarization levels. In any horn, the antenna pattern is severely affected by the diffraction from the edges which can lead to undesirable radiation not only in the back lobes but also in the main lobe. By making grooves on the walls of the of a horn, the spurious diffractions are eliminated. Such horns are called "*Corrugated horns*"[4]. Our feed at 1420 MHz. has fins instead of grooves, since the whole assembly is made out of brass sheets. The flare–angle of the horn is $120°$. The dimensions of the feed are:

- Aperture diameter : $3.65\,\lambda$
- Horn length : $4.48\,\lambda$

The phase center has been found out to be at the apex of the cone - at a depth of 200 mm from the aperture plane. This feed has an impressive bandwidth: 580 MHz, starting from 1000 MHz to 1580 MHz, as can be seen from Fig 19.15

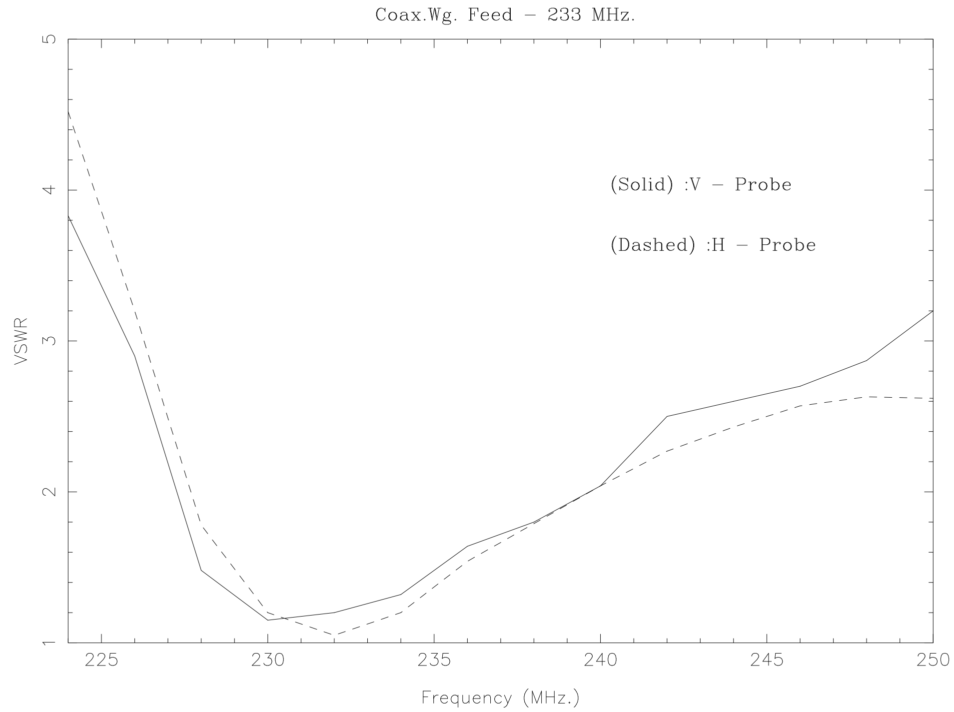

Figure 19.14: The VSWR as a function of frequency for the 233 MHz feed.

Radiation patterns, including the cross-polar pattern is shown in Fig 19.16.

The edge taper is -19 dB and the cross-polar peak is -24 dB. The front-end electronics is housed in a rectangular box,on the back side of the horn, forming one integral unit. The entire band is divided into 4 subbands, each 140 MHz wide and centered on 1390, 1280, 1170 and 1060 MHz. There is also a bypass mode in which the entire bandwidth is available.

19.8 GMRT Antenna Efficiencies

The efficiency relations shown in Section 19.5, have not considered the effect of aperture blockage by feeds and feed-support frames ("*quadripod legs*" in GMRT–parlance). Simple geometrical optics based models for such computation exist,[16] which are used along with GMRT–specific efficiency relations, to produce the following table. Limitations of this model are highlighted in [17].

Some of the loss terms can be expressed as equivalent noise temperatures (see Chapter 3). The spillover temperature is given by (see also Eqn 19.4.14)

$$T_{Sp} = T_g \cdot \frac{\int_{\theta_0}^{\pi/2} |E(\theta)|^2 \sin(\theta) d\theta}{\int_0^{\pi} |E(\theta)|^2 \sin(\theta) d\theta} \tag{19.8.25}$$

where T_g is the ground temperature. Considering the reflectance of soil at microwave frequencies, it is presumed as 259° K.

Similarly, the mesh–leakage T_{ml}, scattered radiation by the feed– support frames T_{sc}, can also be expressed in terms of T_g. The overall system temperature (see Chapter 3) is

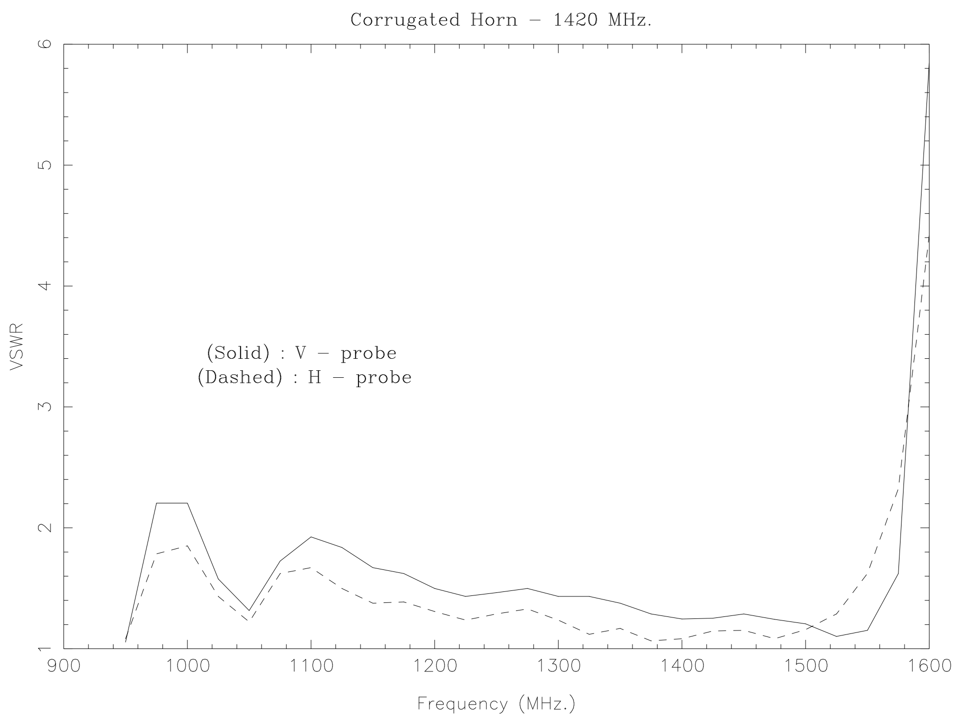

Figure 19.15: The VSWR as a function of frequency for the 1420 MHz feed.

the sum of all these and the receiver noise temperature, T_r and the sky temperature,T_{sky}, which is assumed to be,

$$T_{sky} = 3.0 + 20{\cdot}(408/f)^{2.75}, \qquad (19.8.26)$$

where f is the frequency of the received signal (in MHz). Hence

$$T_{sys} = T_r + T_{sky} + T_{Sp} + T_{ml} + T_{sc}. \qquad (19.8.27)$$

Finally the figure–of–merit of any radio antenna, is the gain-by-system temperature ratio, G/T_{sys}, expressed as :

$$G = \frac{SA_p\eta_a}{2k}, \qquad (19.8.28)$$

where S is flux density in units of Jansky, A_p, is the physical area of the parabolic dish and η_a is the overall aperture efficiency. For a 1 Jy. source at the beam of the antenna and value of Boltzmann's constant k included in the above relation,

$$G = \frac{A_p\eta_a}{2760}. \qquad (19.8.29)$$

Hence, the ratio G/T_{sys} is expressed in units of Jy^{-1}.

A summary of the relevant parameters for the GMRT antennas is given in Table 19.4. These have been computed based on the following assumptions.

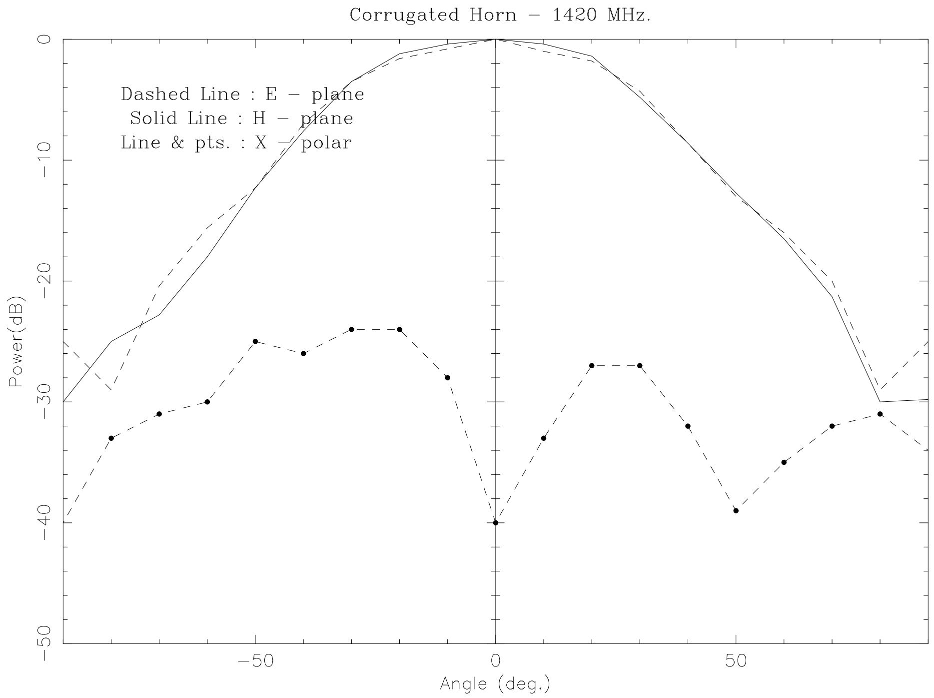

Figure 19.16: Radiation Pattern of the 1420 MHz feed.

1. $T_r = 100°$ K for 150,233 and 327 MHz bands; $50°$ K for 610 MHz and $35°$ K for the 1000 to 1400 MHz bands.

2. The surface rms, $\sigma_1,\ \sigma_2,\ \sigma_3$ values are 8.0, 9.0, and 14.0 mm respectively.

The agreement between the observed HPBW, gain and system temperature and the computed values is in general quite good.

19.9 Further Reading

1. Swarup, G., Ananthakrishnan, S., Kapahi, V.K., Rao, A.P., Subrahmanya, C.R., and Kulkarni, V.K., 'The Giant Metre-wave Radio Telescope', Current Science, Vol.**60**, No.2, (1991).

2. Chengalur, J.N., Kher, R.K. 'Transmission through Wire Grids', TIFR Internal Report, 1987.

3. Kaplun, V.A., Babkin, N.I., Goryachev, B.G., 'Shielding Propeties of Wire Screens at SHF', Radio Engg. & Elec. Physics, **9**, (1964), pp.1428–30.

4. Clarricoats, P.J.B., and Olver, A.D., Corrugated horns for Microwave Antennas, Peter Peregrinus Ltd., London, (1984)

5. Stutzmann, W.L., and Thiele, G.A., Antenna Theory & Design, John Wiley & Sons. Inc., (1981)

	Frequency (MHz)						
Eff.	150	233	327	610	1000	1200	1400
Tap Eff.	0.689	0.823	0.715	0.775	0.566	0.533	0.592
Spill. Eff.	0.952	0.799	0.944	0.835	0.967	0.971	0.971
Mesh Eff.	0.999	0.999	0.998	0.991	0.943	0.941	0.94
RMS Eff.	0.997	0.992	0.986	0.948	0.88	0.835	0.78
Aper. Eff.	0.652	0.651	0.664	0.608	0.452	0.405	0.422
Tsys($^\circ$ K)	428	229	152	92	65	77	62
$\frac{G}{T_{sys}} \times 10^{-3}$	0.877	1.64	2.53	3.81	4.04	3.02	3.17
$HPBW$	2° 52'39"	1° 51'06"	1° 21'15"	0° 42'48"		0° 19'26"	

Table 19.4: Calculated aperture efficiencies and system temperatures for the GMRT antennas.

6. Kildal, P-S., "Factorization of the Feed Efficiency of Paraboloids and Cassegrain Antennas", IEEE Trans.on Ant.& Propg., Vol.**AP-33**, No.8, (1985).

7. Krishnan, T., "Analysis of TIFR / GMRT 45 m. dish performance at 327 MHz.", HAE/HSS Report 010/92, Sept.1992.

8. Sankar, G., Swarup, G., Ananthakrishnan.S., Sankararaman, M.R., Sureshkumar .S. and Izhak.S.M. "Prime focus feeds for GMRT Antenna"IAU - 6th Asian Pacific Regional Meeting on Astronomy, IUCAA, Pune. Aug.1993.

9. Guillou.L., Daniel.J-P., Terret.C., Madani.A., "Rayonnement d'un Doublet Replie Epais", Annales des Telecommunications, tome 30, nr 1-2.

10. Kildal, P-S., and Skyttemyr, S.A., "Dipole-Disk Antenna with Beam-Forming Ring", IEEE Trans.on Ant.& Propg., Vol.**AP-30**, No.4, (1982).

11. Livingston, M.L., "Multi-frequency Coaxial Cavity Apex Feeds", Microwave Journal, (Oct.1979) pp.51–54.

12. Van Ardanne, A., Bregman, J.D., Sondaar, L.H., Knoben, M.H.M., "A Compact Dual Polarized Coaxial Feed at 327 MHz.", Electronics Letters, Vol.**20**, No.18, (1984) pp.723–724.

13. Jeuken, M.E.J., Knoben, M.H.M, and Wellington, K.J., "A Dual Frequency, Dual Polarized Feed for Radioastronomical Applications", Rechnernetze und Nachrichtenverkehrstheorie, NTZ, Heft:**8**, (1972) pp.374–376.

14. Shafai, L. and Kishk, A.A., "Coaxial Waveguides as Primary Feeds for Reflector Antennas and comparison with Circular Waveguides", AEÜ, Band:**39**, Heft 1, (1985) pp.8–14.

15. Sankar, G. and Praveenkumar, A., "Dual Frequency Coaxial Waveguide Feed - Design calculations", Int.Tech.Report, **AG-02/90**, GMRT–TIFR, Pune.

16. Fisher, J.R., "Prime-focus Efficiency, Blockage, Spillover and Scattering Calculations on the HP 9825A Calculator", EDIN Report.174, NRAO, Nov.1976.

17. Chengalur, J.N. "Aperture Efficiency Calculations for GMRT Dishes", NCRA-TIFR Int.Tech.Report, Dec.1993.